Vehicular Communications 34 (2022) 100456

Contents lists available at ScienceDirect

Vehicular Communications

www.elsevier.com/locate/vehcom

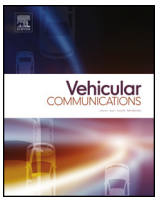

Adaptive beamwidth optimization under Doppler ICI and positioning errors at mmWave bands

Christian Ballesteros [a,*], Andreas Pfadler [b], Luca Montero [a,c], Jordi Romeu [a], Luis Jofre-Roca [a]

[a] Universitat Politècnica de Catalunya (UPC), Jordi Girona 31, Barcelona, 08034, Spain
[b] Volkswagen Commercial Vehicles, Hermann-Münch-Straße 1, Wolfsburg, 38440, Germany
[c] SEAT S.A., A-2, KM. 585, Martorell, 08635, Spain

ARTICLE INFO

Article history:
Received 15 September 2021
Received in revised form 3 December 2021
Accepted 19 January 2022
Available online 24 January 2022

Keywords:
V2N
Beamforming
Arrays

ABSTRACT

The growing trends towards massive antenna arrays with focusing capabilities has enabled the use of higher frequencies at the cost of more complex systems. In the particular case of vehicular communications, millimeter-wave (mmWave) communications are expected to unleash a set of advanced use cases with stringent spectrum needs. However, dealing with very directive patterns and high frequencies entail additional challenges such as beam misalignment and Doppler effect. This paper presents a beam optimization procedure for vehicle-to-network (V2N) systems in which a base station communicates with high-speed users. Aided by the a priori knowledge of the vehicle location, the base station is able to estimate the average signal-to-interference-plus-noise ratio (SINR) until the next beam refresh considering the positioning accuracy and the Doppler inter-carrier interference (ICI). The estimation includes the antenna beamwidth, which can be optimized to maximize the achievable throughput. The numerical results indicate that the SINR can be significantly enhanced compared to beam sweeping with identical hierarchical codebooks while reducing the probability of outage.

1. Introduction

1.1. Motivation

Vehicles become simultaneously more connected and automated. New applications such as tele-operated driving, HD mapping, platooning, and cooperative driving are essential to enable automated driving. These applications come with stringent requirements on reliability and throughput, which are particularly challenging in high mobility scenarios. In general, one refers to quality of service (QoS) requirements, such as latency, data rate, and reliability [1,2]. It is foreseen that connected vehicles will require more spectrum than provided nowadays. Even the recent roll-out of the 5th generation cellular system (5G) in sub-6 GHz, i.e., frequency range one (FR1), does not satisfy the spectrum need of connected vehicles together with the increasing cellular user demand [3]. Therefore, research focuses on the use of mmWave bands. In particular, appropriate beamforming strategies addressing the QoS requirements in vehicular networks are essential and investigated in this paper.

Operating at mmWave bands requires the use of beamforming techniques to cope with inherent additional losses [4,5]. This brings a few challenges with it, especially in vehicular scenarios. The authors highlighted in [6] the importance of massive antenna geometries in vehicle-to-infrastructure (V2I) based on the analysis of the channel capacity and eigenvalues, also emphasizing the need of adequate beam refreshing times. Similarly, in [7], the use of singular value decomposition (SVD) precoding is compared to maximum-ratio combining (MRC) and pre-defined codebooks in terms of SINR for a given highway scenario. The peculiarities of highway and urban V2I can be found in [8] and in [9], respectively. The former presents very high probability of line of sight (LOS) with small angular spread of multipath components, whereas the coverage of a base station (BS) in the latter case is much degraded due to the grid-like shape of the streets.

The use of highly directive beams also intends to reduce the interference between users and increase the energy efficiency, at the cost of higher beam update rates and signaling. To provide reliable focusing, accurate channel state information and/or user positioning needs to be exchanged. In case of mmWave channels, some experiment-based models are discussed in [10,11] that allow the prediction of the behavior of such type of links under realistic circumstances. However, accurate and real-time channel state updates

* Corresponding author.
E-mail address: christian.ballesteros@upc.edu (C. Ballesteros).

https://doi.org/10.1016/j.vehcom.2022.100456

are crucial in rapidly varying links to allow reliable communications, which is paramount in safety-related applications. The angular and temporal correlation of the channel is discussed in [12] for different sub-6 GHz and mmWave frequencies, with sparser multipath components as the frequency increases. Doppler effects may also cause significant impairments leading to beam steering inaccuracy [13,14].

Location-based beamforming strategies require precise information of the users position, which is not always achieved. In the particular case of vehicles, several positioning technologies are available, such as: cellular trilateration [15], GNSS [16], or joint in-band position prediction [17]. The advent of 5G also promises enhanced positioning features [18] with expected positioning errors in the order of tens of centimeters.

In [19], the main use cases and challenges of beam management in vehicular scenarios are presented. The procedure can be partitioned into two parts: First, the beam alignment phase, where the beams from both sides need to be aligned to establish a communication link. Second, the beam management strategy including user tracking and refinement of beams. The collective knowledge of the vehicles' trajectory allows to predict their behavior and optimize tracking and beam selection or adaptation as in [20]. Typically, beam sweeping methods based on hierarchical codebooks reduce signaling overhead and are usually specification-compliant, as in the IEEE 802.15.3c standard [21].

Different from this conventional approach, this paper targets to improve the antenna beamwidth by adapting it according to the positioning quality of the shared vehicle trajectories and the inter-carrier interference caused by Doppler shifts. This approach is particularly useful for those V2N links in which the BS has more sophisticated focusing capabilities and calculation power. Beam sweeping approaches are limited to power measurements, not always a sufficient criterion of quality, and their validity may be short in time. In contrast, using the knowledge of the vehicle trajectory may help to enlarge the refreshing rate of the beams (and, thus, reducing overheads), as well as increase the accuracy of the focusing.

Other previous studies already tackled the problem of beam optimization in vehicle-to-everything (V2X). In [22], a beam-switching strategy of unequal beams covering a highway lane is proposed. The authors consider the vehicle's velocity with timing errors, but other undesired effects in complex environments with realistic radiation patterns are neglected. In [23], a triangular beam pattern modeling the vehicle radiation is optimized with the average capacity for a beam update period. The channel correlation and coherence time are also considered, which limit the validity of the beam and trigger the next update. However, other sources of error are not considered, such as Doppler effect or positioning inaccuracy. More recently, the authors in [24] propose an algorithm for beamwidth optimization in vehicle-to-vehicle (V2V) highway scenarios. They consider the misalignment due to positioning errors in the azimuth plane and the effect of surrounding users with a Montecarlo-based optimization of the entire system. The work presented in the current manuscript proposes a novel beamforming strategy for BS-to-vehicle systems. Assuming an orthogonal frequency division multiplexing (OFDM)-like communication, an expression of the SINR in presence of the Doppler ICI due to the vehicle motion is obtained using the channel correlation. In this case, the location of the target vehicle is assumed to be known with a certain accuracy, which is also used in the calculation of the desired and self-interference signal. Then, the average SINR until the next beam update is maximized for a given set of available beamwidths. The proposed strategy is studied for a large group of randomly distributed users and compared with the expected performance in typical beam sweeping strategies.

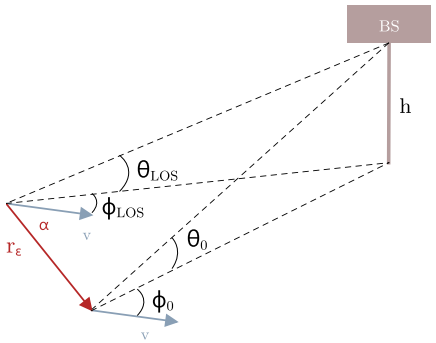

Fig. 1. Steering errors due to inaccurate positioning and vehicle movement.

1.2. Scope of the study

In this section, the scope of the paper is presented. The main contributions can be summarized as follows:

- Proposing a novel beamforming strategy to optimize throughput with a certain confidence level taking into account the vehicle position inaccuracy and speed.
- Considering Doppler effect and vehicle speed in the optimization. Wider beamwidths are prone to larger Doppler spread. Depending on the probability density function (PDF) of the angle of arrival (AoA) of multipath components at the receiver [25,26], the divergence in Doppler frequency of each multipath degrades the system performance.
- Taking into account the impact of positioning accuracy (relative and absolute position) on the optimum beamwidth, and hence the achievable throughput.
- Simulating V2N channels with realistic beam pattern of the antenna arrays using the QuaDRiGa channel simulator [27].
- Comparing the performance of the proposed method with the widespread beam sweeping strategy, for which some standards already provide resource allocation, e.g., 5G new radio (NR) and IEEE 802.15.3c.

The manuscript is organized as follows: section 2 presents the modeling of the positioning and Doppler, section 3 depicts the equations to obtain the maximization expression of the SINR, section 4 shows the simulated results to validate the proposed strategy, and section 5 concludes the paper with the main outcomes of the work. In addition, an appendix is given at the end with the ICI derivation.

2. System model

2.1. Positioning error modeling

In this paper, the positioning errors of vehicles are modeled following a bivariate distribution including distance and angle around the expected vehicle location in the XY plane. It is common to neglect small errors in height as the vertical beamwidth is assumed wide enough to prevent misalignment's. Typically, two independent and identically distributed Gaussian errors x_ε and y_ε are defined to model the position of the car on the pavement plane. One could also express the positioning error in polar coordinates as $r_\varepsilon \sim \text{Rayleigh}(\sigma_r)$ and $\alpha \sim \text{Unif}(0, 2\pi)$, being r_ε the distance between the estimated and the real positions, and α the angle of the error vector with respect to the driving direction.

Fig. 1 illustrates the relative position with respect to the BS of both the estimated and real vehicle locations. θ_{LOS} and ϕ_{LOS} stand for the expected LOS angles from the vehicle towards the BS, whereas $\theta_0 = \theta_{\text{LOS}} + \Delta\theta\varepsilon$ and $\phi_0 = \phi_{\text{LOS}} + \Delta\phi_\varepsilon$ are the real

angles for the first position of the vehicle trajectory. The steering error in azimuth ($\Delta\phi_\varepsilon$) and elevation ($\Delta\phi_\varepsilon$) is thus calculated as:

$$\begin{aligned}\tan\Delta\phi_\varepsilon &= \frac{\sin(\phi_{\text{LOS}}-\alpha)}{\frac{\tilde{D}}{r}-\cos(\phi_{\text{LOS}}-\alpha)}\\ \tan\theta_0 &= \tan\theta_{\text{LOS}}\frac{\sin(\phi_0-\alpha)}{\phi_{\text{LOS}}-\alpha},\end{aligned} \tag{1}$$

where $\tilde{D}=D\cos\theta_{\text{LOS}}$ is the distance from the BS to the car in the XY plane. All azimuth angles are referred to the driving direction defined by the velocity vector.

Following the same approach, one can calculate the beam misalignment due to the vehicle motion. In this case, the error vector is replaced by the distance traveled by the car from its initial position. The angle between the error vector and the velocity vector is now zero. The error when estimating the velocity is assumed to be negligible. Its impact is expected much lower than the actual positioning and the information is updated so often that any change in the traveling direction is not substantially degrading the estimation.

Then, the azimuth ($\Delta\phi$) and elevation ($\Delta\theta$) misalignment from its initial position follow these expressions:

$$\begin{aligned}\Delta\phi &\simeq \frac{v\tau\sin\phi_0}{D_0\cos\theta_0 - v\tau\cos\phi_0}\\ \Delta\theta &\simeq \frac{\delta-\tan\theta_0}{1+\delta\tan\theta_0},\end{aligned} \tag{2}$$

where $\delta\simeq {}^{h\Delta\phi}/_{v\tau\sin\phi_0}$ and v is the magnitude of the velocity vector. It is worth mentioning that small angle approximations ($\sin x\simeq x$, $\cos x\simeq 1$) have been used in the previous expressions given the small error due to the movement, since the beam and vehicle dynamics update rate are considerably faster than any noticeable change in its motion.

2.2. Doppler effect on ICI

The use of multi-carrier modulation schemes such as OFDM introduces a higher degree of robustness against channel dispersion. Long symbol duration is additionally compensated by a redundant cyclic prefix (CP) and multipath delay spread is thus mitigated. However, OFDM systems tend to lose the orthogonality between subcarriers in fast time-variant scenarios. This is the case of vehicular communications. High speeds introduce large Doppler shifts that may severely degrade the signal quality. In V2V, where two or more vehicles exchange information using direct sidelink communications, Doppler represents a major challenge. Very directive beams can alleviate this effect. A direct relation between beamwidth and Doppler spread is demonstrated in [25,26]. Conversely, thanks to the powerful focusing capabilities of next generation cellular stations, one could exploit the use of large arrays to mitigate the Doppler effect and also increase the power on the user's side. This is the case of V2N communications, where a cellular base station is linked to a vehicle using downlink and uplink streams. This work tries to address this situation in the following sections.

In [28], a statistical analysis of the ICI under the wide-sense stationary uncorrelated scattering (WSS-US) assumption is performed. The study also assumes Rayleigh fading but the channel is modeled in terms of a two-dimensional correlation function. Additionally, the authors in [29] present the temporal evolution of vehicular beamformed channels. This is later used to obtain the channel coherence time and a novel parameter such the beam coherence time, which can be related to a larger beam refresh. The work in [28,29] is thus used as baseline in the following sections to derive the actual power of the ICI in beamformed V2N channels. The derivation is extended to a full 3D scenario in which a cellular BS optimizes its focusing towards a moving vehicle.

3. Optimum beamwidth analysis

3.1. Beamforming channel model

Given a wideband frequency selective channel, one can divide its impulse response for each OFDM k-th subcarrier to be $h_k(t,\tau)$. This response is zero-mean and stationary for all N subcarriers, with cross covariance between sub-channels $h_k(t,\tau)$ and $h_l(t,\tau)$ expressed as:

$$R_{h_k,h_l}(\tau)=\mathbb{E}[h_l(t)h_k^*(t+\tau)];\ k,l=1,...,N. \tag{3}$$

Assuming that the channel follows a WSS-US, the correlation function is factorable as follows [28,30]:

$$R_{h_k,h_l}(\tau)=R_1(\tau)R_2(k-l), \tag{4}$$

where $R_1(\tau)$ is the delay correlation and $R_2(k-l)$ the correlation between subcarriers. The first term is directly related to the Doppler spectrum, which cannot be assumed to follow a Clarke-Jakes distribution [31,32]. In this case, the delay correlation function, $R_1(\tau)$, can be split into LOS and non-line of sight (NLOS) terms, being the first one related to the pointing direction whereas the second one is assumed to follow the one-ring scatterer model as in [29]:

$$\begin{aligned}R_1(\tau)&=\mathbb{E}[h_k(t)h_k(t+\tau)]\\ &=\frac{K}{K+1}R_{\text{LOS}}(\tau)+\frac{1}{K+1}R_{\text{NLOS}}(\tau),\end{aligned} \tag{5}$$

where K is the Rician factor relating the power of LOS and NLOS components.

The channel correlation is also depending on the chosen antenna pattern for such scenarios. Following the same approach as in [29], the analytical expressions used for beam optimization make use of the von Mises distribution to model the beamforming gain. In this paper, the bivariate von Mises distribution is used as a model for the azimuth and elevation gain [33]. For two uncorrelated variables, the expression of the antenna gain reduces to:

$$G(\theta,\phi|\mu_\theta,\mu_\phi)=G_0e^{k_\theta\cos(\theta-\mu_\theta)+k_\phi\cos(\phi-\mu_\phi)}, \tag{6}$$

where G_0 is a normalization variable related to the maximum gain, μ_θ and μ_ϕ represent the elevation and azimuth steering angles and $k_\theta\approx 1/\theta^2_{-3\,\text{dB}}$ and $k_\phi\approx 1/\phi^2_{-3\,\text{dB}}$ are the concentration parameters of the bivariate von Mises distribution that are inversely proportional to the squared half-power (-3 dB) beamwidth for highly directive antennas.

$$\begin{aligned}&R_{\text{LOS}}(t,\tau)\\ &=\mathbb{E}\Bigg[\frac{\big(G(\theta_0,\phi_0|\theta_{\text{LOS}},\phi_{\text{LOS}})G(\tilde{\theta},\tilde{\phi}|\theta_{\text{LOS}}+\Delta\theta,\phi_{\text{LOS}}+\Delta\phi)\big)}{G_{\max}\exp\{k_\theta+k_\phi\}}\\ &\quad\times\exp\{j2\pi f_D t\big(\cos\theta_0\cos\phi_0-\cos(\theta_0+\Delta\theta)\cos(\phi_0+\Delta\phi)\big)\}\\ &\quad\times\exp\{-j2\pi f_D\tau\cos(\theta_0+\Delta\theta)\cos(\phi_0+\Delta\phi)\}\Bigg]\end{aligned} \tag{7}$$

In (7), the LOS correlation is presented. Once normalized to the maximum achievable gain, two phase terms appear: one depending on time and one depending on delay. The former can be neglected since $\Delta\theta$ and $\Delta\phi$ are assumed to be very small (proportional to the delay). The correlation thus is not dependent on time and the wide-sense stationarity is fulfilled. The second phase

term depends both on the initial positioning error and that small angular shift due to the movement in τ. The equation can be then simplified to the expression in (8).

Due to the inherently directive nature of beamforming mmWave links [34], those incoming paths close to the LOS component are expected to have a much higher impact on the perceived signal at the receiver. Therefore, for the sake of simplicity in the analysis, only the LOS correlation term is assumed from now on ($K \gg 1$). In any case, this simplification only affects the beam optimization function and not the numerical analysis carried out in the following chapters, since all multipath components are considered when calculating the channel performance. In consequence, the delay-term of the correlation from the initial position onward can be expressed as in (8).

$$\begin{aligned} R_1(\tau) &\simeq R_{\mathrm{LOS}}(\tau) \\ &\simeq \mathbb{E}\Bigg[\exp\Big\{ k_\theta \Big(\cos\Delta\theta_\varepsilon + \frac{\Delta\theta}{2}\sin\Delta\theta_\varepsilon - 1 \Big) \\ &\quad + k_\phi \Big(\cos\Delta\phi_\varepsilon + \frac{\Delta\phi}{2}\sin\Delta\phi_\varepsilon - 1 \Big) \Big\} \\ &\quad \exp\Big\{ -j2\pi f_D \tau \cos\Big(\theta_0 + \Delta\theta\Big)\cos\Big(\phi_0 + \Delta\phi\Big)\Big\}\Bigg] \end{aligned} \tag{8}$$

The power delay profile (PDP) is assumed to be exponential, as in a tap delay model, in the form $\mathrm{PDP}(\tau) = \frac{1}{\sigma_\tau}\exp(-\frac{\tau}{\sigma_\tau})$, with $\tau \geq 0$. In this expression, σ_τ represents the delay spread, which can be translated to the channel coherence bandwidth. By calculating the Fourier transform of the PDP, one can obtain the correlation over the frequency, $R_H(f)$. The sampled frequency correlation at every subcarrier corresponds to the second term in (4), $R_2(k) = R_H(k\Delta f)$. Thus, the relation between the PDP and $R_2(k)$ can be summarized as:

$$R_2(k) = \frac{1}{\sigma_\tau}\int_0^\infty e^{-\frac{\tau}{\sigma_\tau}} e^{-j2\pi k\Delta f\tau} d\tau = \frac{\kappa}{\kappa + j2\pi k\Delta f}, \tag{9}$$

where $\kappa = 1/\sigma_\tau$.

3.2. Received signal and SINR

The received signal at the user terminal is:

$$r(t) = h(t,\tau) \circledast s(t) + n(t), \tag{10}$$

where $s(t)$ is the baseband signal at the transmitter and $n(t)$ stands for additive Gaussian noise. The symbol $\circledast$ denotes the convolution operation.

Assuming a slow-fading subcarrier channel (i.e., the symbol period is much smaller than the coherence time [6,29]), the symbols detected at the output of the k-th subcarrier of the OFDM receiver can be expressed as [28]:

$$\hat{x}_k = h_k(t_0)x_k + \frac{NT}{2\pi j}\sum_{\substack{l=1 \\ l\neq k}}^{N} \frac{h_l'(t_0)x_l}{l-k} + n_k, \tag{11}$$

where T is the symbol period ($T = \frac{1}{\Delta f}$), x_k is the original symbol sent at the k-th subcarrier and n_i is the Gaussian noise after the correlator with zero mean and N_0 power density.

In the Appendix, details about the calculation of the SINR accounting for ICI in beamforming environments are provided. Then, the SINR at each subcarrier can be expressed as:

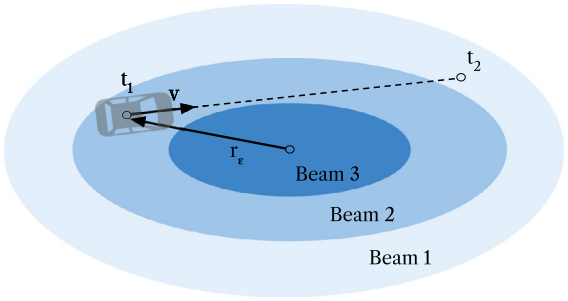

Fig. 2. Sketch of the vehicle position relative to the beam spot.

$$\mathrm{SINR}_k = \frac{P}{P|R_1''(0)|\left(\frac{NT}{2\pi}\right)^2 \sum_{\substack{l=1 \\ l\neq k}}^{N} \frac{1}{(l-k)^2} + N_0 B}. \tag{12}$$

As stated in (12), the SINR must be defined for each subcarrier. When accounting for those in-band fluctuations, $\mathrm{SINR}_{\mathrm{eff}}$ can be used as an abstraction from multi-carrier instantaneous measures to a single value that allows to evaluate the link-level performance from a system perspective. In [35], further details about the calculation of the $\mathrm{SINR}_{\mathrm{eff}}$ for OFDM systems are provided. The authors provide up to four different effective SINR mapping models for it calculation from the sub-carrier individual SINR values. Nonetheless, the links in the system experience less multipath components thanks to the inherent directivity of mmWave bands given the large attenuation of some multipath components, further increased by the use of sharp beams. Those components far from the angular region covered by the beam are severely attenuated, which translates to larger beam coherence times and smaller in-band SINR fluctuations. In that regard, and targeting to a low-complex implementation under realistic circumstances, the $\mathrm{SINR}_{\mathrm{eff}}$ calculation is approximated to the average among all the individual SINR values per subcarrier.

$$\mathrm{SINR}_{\mathrm{eff}} \approx \sum_{k=1}^{N} \mathrm{SINR}_k \tag{13}$$

3.3. Beam outage and link stability

High-mobility environments are prone to fast changes in the wireless channel characteristics. In the case of beamforming systems, steering information must be rapidly updated to provide an accurate enough tracking of the target. This information is also affected by prediction inaccuracies worsening the quality of the link. Beam recovery strategies must be provided to prevent beam-steering algorithms to lose track but this is left out of the scope of the present work.

Given a beam with $\theta_{3\,\mathrm{dB}}$ and $\phi_{3\,\mathrm{dB}}$ beamwidth in elevation and azimuth, respectively, the probability of falling outside its -3 dB footprint, also coined here as beam outage, is expressed as:

$$P_{bo} = 1 - \int_{\mu_\theta - \frac{\theta_{3\,\mathrm{dB}}}{2}}^{\mu_\theta + \frac{\theta_{3\,\mathrm{dB}}}{2}} \int_{\mu_\phi - \frac{\phi_{3\,\mathrm{dB}}}{2}}^{\mu_\phi + \frac{\phi_{3\,\mathrm{dB}}}{2}} f_{\theta,\phi}(\theta,\phi)\,d\theta\,d\phi, \tag{14}$$

where μ_θ and μ_ϕ are the steering angles of the beam in elevation and azimuth and $f_{\theta,\phi}(\theta,\phi)$ is the joint density function of the vehicle position based on the definitions in Section 2.1.

The definition of beam outage does not directly relate to actual outage or reliability but it might be used as a hint of the suitability of a certain beam. Fig. 2 illustrates the position of a vehicle with respect to the beam spot for a given positioning accuracy for

a certain trajectory within the time period between t_1 and t_2. It is assumed that the BS beam uses the closest beam to the expected position of the vehicle. Higher speed or larger positioning inaccuracy might lead to a wrong beam choice and hence reducing dramatically the perceived signal. This issue can be alleviated by increasing the beamwidth at the expense of reduced gain.

3.4. Beamwidth optimization

The target vehicle reports its position and velocity every T_v seconds. In parallel, the BS updates its beam with a T_b periodicity. In case of typical beam sweeping strategies, this would represent that all beam combinations are swept every T_b seconds, for instance, by means of synchronization signal block (SSB) bursts in 5G NR.

Since the proposed strategy is a single-side optimization algorithm, the BS makes use of the most recent vehicle information to predict the current position and driving direction. A safety margin due to positioning inaccuracies is considered by assuming that the standard deviation of the positioning error distribution is known. Thus the optimization is based both on the achievable channel capacity and the probability of the car to lay outside the beam footprint (beam outage).

The optimum beamwidths in elevation and azimuth ($\theta^{\text{opt}}_{\text{-3 dB}}$, $\phi^{\text{opt}}_{\text{-3 dB}}$) are chosen to maximize the overall data transmission for each beam period, T_b. In the optimization process, two simultaneous goals are pursued: minimize the outage probability and maximize the channel capacity (i.e., throughput). The abrupt degradation of the signal outside a beam coverage area makes the first goal almost a must, which also tightly relates to the second one. Data delivered outside the beam boundaries should be left as marginal, triggering an update of the beam for the next period in case that the vehicle is outside that area. Furthermore, accounting for involuntary data reception outside the beam coverage may lead to a suboptimal use of resources. Then, the optimization function can be written as:

$$\theta^{\text{opt}}_{\text{-3 dB}}, \phi^{\text{opt}}_{\text{-3 dB}} = \arg\max_{k_\theta, k_\phi} \int_0^{T_b} (1 - P_{\text{bo}}) \log_2(1 + \text{SINR}_{\text{eff}}) \, , \qquad (15)$$

which includes the effective SINR (SINR_{eff}) and the beam outage probability as parameters.

Given a set of pre-defined beamsets, with different azimuth and elevation beamwidth for their individual beams, the closest beam to the expected LOS is chosen for each. The optimum one from this subset of beams is chosen based on the maximization criterion in (15). This approach tackles a complex optimization problem with a simple, yet feasible way for massive deployment with multiple vehicles under real-time coverage.

4. Numerical evaluation

The proposed optimization strategy is then validated through numerical simulations. A set of N_v vehicles is randomly distributed within the coverage area of a BS. Each one is independently simulated assuming a linear trajectory with a constant speed, v, during T_t seconds. Once the trajectory of the current vehicle is simulated, the results are stored and the next vehicle is dropped to the scenario. The car positions are sampled every Δt seconds and all values (e.g., SINR, outage) are computed for each sample. LOS visibility is assumed for all users, following the channel model proposed by the 3rd Generation Partnership Project (3GPP) for highway scenarios in [36]. In that regard, the QUAsi Deterministic RadIo channel GenerAtor (QuaDRiGa) libraries are used to retrieve the channel impulse response along each trajectory [27]. The results discussed below are based on the averaged values for all computed trajectories to obtain suitable statistics. Fig. 3 depicts the simulation scenario for a given vehicle trajectory.

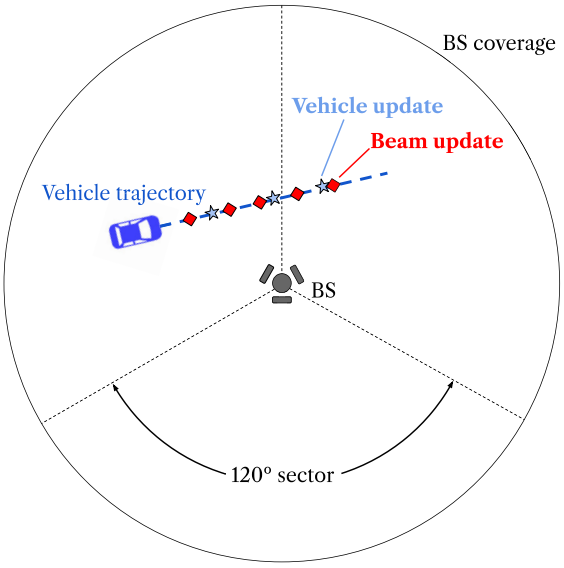

Fig. 3. Simulation scenario with a single vehicle. The update of the vehicle information and the BS beam is illustrated along the trajectory.

Table 1
Parameters used for the simulation.

Parameter	Symbol	Value
Carrier frequency	f_c	28 GHz
Channel bandwidth	B	50 MHz
Transmission power	P_T	20 dBm
Channel model		Highway LOS [36]
Number of vehicles	N_v	500
Max BS-vehicle distance		300 m
Velocity	v	{25, 50, 100, 150, 200} km/h
Total simulation time	T_t	5 s
Sampling interval	Δt	0.01 s
Beam update period	T_b	{20, 40, 80, 160} ms
Vehicle positioning period	T_v	200 ms
Number of sectors	N_s	3
Azimuth sector		$[-60, 60]^\circ$
Elevation sector		$[-60, 30]^\circ$
Number of beamsets	N_b	3
Azimuth beamwidth	$\phi_{\text{-3 dB}}$	$\{24, 12, 6\}^\circ$
Elevation beamwidth	$\theta_{\text{-3 dB}}$	$\{50, 24, 12\}^\circ$

The BS is composed by N_s equal sectors covering the entire azimuth range. It calculates the optimum beam with T_b periodicity and the vehicle reports its (randomly erroneous) position every T_v seconds. Up to N_b beamsets are considered at the BS, choosing the closest beam towards the car for each of them. The N_b beams are then evaluated in terms of the expressions in Section 3.4. Then, every T_b, the process is triggered again with the most recent information of the car. Table 1 lists the different simulation parameters.

When evaluating the suitability of a beam, one can follow several criteria. Typically, beam sweeping strategies are based on power measurements carried out by the receiver when the transmitter sends some signaling messages with a finite set of beams. Nevertheless, the beam with the highest power is not always the one with the best performance in terms, for example, of SINR – tightly related to throughput and error rates. On the other hand, repeated messaging with several beams leads to an increased overhead and larger periods of time to retrieve the optimum beam. In addition, the "instantaneous" measurement of such beams re-

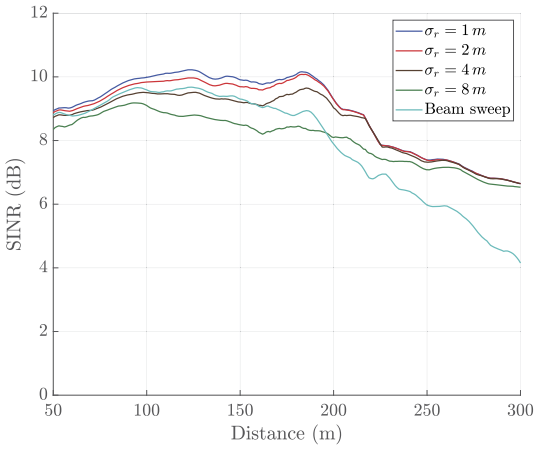

Fig. 4. SINR against LOS distance between the BS and the vehicles.

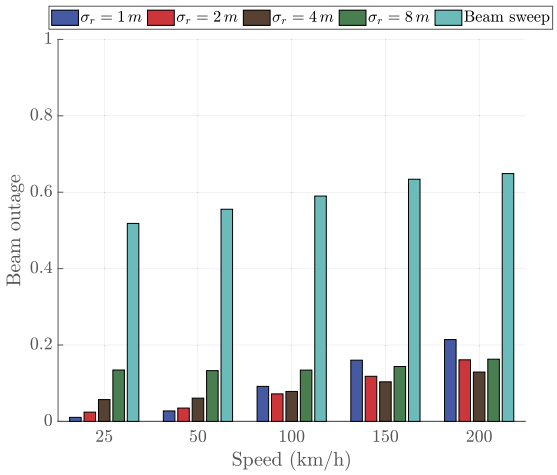

Fig. 5. Beam outage for different speed and standard deviation of the positioning error values.

quires fast refresh rates so they are valid enough until the next update. The proposed approach only makes use of the position and speed information from the receiver, which is periodically reported but at a much lower rate with very low associated overhead. The position and speed information can even be sent in a separate channel at lower frequencies. The use of optimization algorithms to retrieve the optimum beamwidth is also discarded due to its complex application in realistic scenarios. However, the presented methodology later compared to some optimization algorithms with a subset of vehicles to prove that the benefit-cost ratio is quite low when compared with the proposed approach. The authors propose to substitute current beam sweeping stages by a single-message exchange from the vehicle to the base station and fast SINR calculations using existing codebooks with the previous expressions.

The performance of such approach is thus compared to a typical hierarchical beam sweeping strategy based on periodical power reports from the receiver once the transmitter sends signaling bursts with all possible beams. It is decomposed in two phases. First, a low-directivity set of beams is evaluated, corresponding to the so called beam determination stage. The next beam update period is used for beam refinement, in which a set of narrower beams is used. The limit in the number of beams to sweep within a T_b interval defines the maximum number of neighboring beams to test so they still fulfill the requirements of current standards as in 5G NR, which limits the signaling blocks to 64 per burst in the case of frequency range two (FR2) [37]. The beamwidth is reduced until the highest hierarchy is reached. Then, only neighbor beams are swept until the vehicle exceeds the coverage of a sector, where the low-level beams are swept again and the process starts again. All beams are swept at the lowest level to allow the BS to find the car regardless its position. A fixed number of 5 neighbors per dimension (25 in total) are swept at higher levels.

4.1. SINR evolution

There are two main parameters that influence the optimization as previously stated: the vehicle speed and the accuracy of the positioning method, defined by the standard deviation of the positioning error (σ_r). In this section, the evolution of the SINR is studied for different cases in terms of those parameters. For instance, Fig. 4 depicts the SINR as a function of the distance between the vehicle and the BS for several positioning error values, i.e., standard deviation of the Rayleigh distribution. All vehicles drive at a constant speed of 100 km/h and the beam is updated every 40 ms.

As expected, the divergence between lines in Fig. 4 is reduced as the distance increases and the angular error becomes similar. For relatively short distances, the additional path losses are overcome with more directive beams. The performance of the beam sweeping strategy in terms of SINR is similar to the proposed solution, even better for very high positioning errors, until 200 m. The use of the most directive beams during almost the entire trajectory leads to much probable outage locations and this has an big impact in the statistics when power is comparable to noise. In addition, the change in the trend of all curves coincides with those distances for which the received power is so low that the ICI becomes much lower than the noise and propagation losses have a direct impact on the SINR.

4.2. Misalignment and gain loss

Optimized beams consider both channel capacity and beam outage probability. Therefore, it is a matter of interest to capture the evolution of the latter under various conditions. In this case, the simulated trajectories are limited to a coverage area of 200 m in which small positioning errors are still meaningful. It is also typical that highly demanding applications in terms of throughput as the ones offered by mmWave V2X are limited to a relatively small cell coverage.

The probability of the car to be outside the footprint of the chosen beam is as illustrated in Fig. 5. The values are given for speeds between 25 and 200 km/h and deviations of the vehicle position from 1 to 8 m. In light blue, the beam outage probability for the beam sweeping case is also shown. The consideration of the vehicle positioning (with a certain accuracy) really helps the BS to avoid large outage periods as seen in Fig. 5. The fact that finer beams are used for low σ_r values implies slightly larger loss in SINR. When the car speed is increased, this difference of using narrow (low σ_r) and wide beams (high σ_r) is more noticeable. However, the achievable SINR evolves as expected (Fig. 4). The average SINR degradation due to outage is much lower than the one due to the use of wider beams when the positioning error becomes higher. Targeting to provide accurate QoS for advanced vehicular use cases at mmWave bands, alternative optimization methods should be investigated to minimize the impact of outage.

Moreover, one could expect that outage increases both with the positioning error and the vehicle speed. For the former, this is true for relatively low speeds. However, this trend is not kept from 100 km/h forward. To understand this effect and provide a plausible explanation, Fig. 6 shows the ratio of usage of each beamset hierarchy level depending on the error. In this case, the velocity is fixed to 100 km/h. It is evident that better positioning allows to

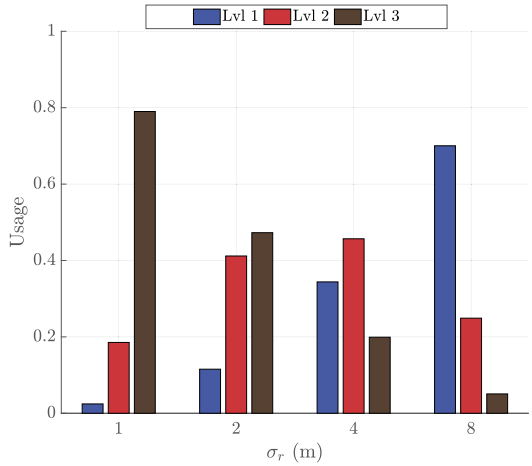

Fig. 6. Beamset hierarchy usage ratio for different values of the standard deviation of the positioning error when driving at 100 km/h.

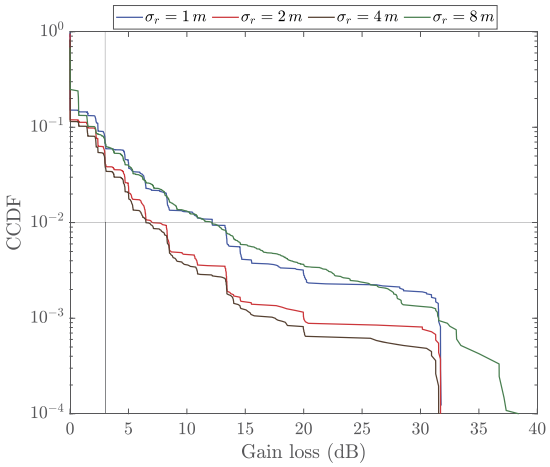

Fig. 7. CCDF of the gain loss due to beam misalignment at 100 km/h. Black lines indicate a 3 dB loss (vertical) and 1% probability (horizontal).

use more directive beams, whereas high errors imply widening the footprint at the expense of less gain.

Finally, the values in Fig. 5 are not directly linked to any reliability metric but they can provide a hint on how effective the energy focusing is. However, the degradation in terms of SINR or packet reception rate (PRR) must be provided for such kind of assessment.

The loss of gain due to beam misalignment is then depicted in Fig. 7. The values are calculated as the difference between the gain of the pattern resulting from the optimization towards the vehicle and the gain of the beam including the LOS direction at the same angles. Again, the speed of the vehicles is 100 km/h. The complementary cumulative distribution function (CCDF) of the gain loss is represented in such a way that one can somehow relate this parameter to a certain reliability level. For instance, regardless of the positioning accuracy, all beams suffer less than 3 dB losses on 94% of the cases. Inversely, with 1% probability, losses will be higher than 6.5 and 12.2 dB for $\{2, 4\}$ and $\{1, 8\}$ m accuracy, respectively.

4.3. Effect of beam update period

Lastly, the impact of the beam update period on the link performance is studied. For the same highway scenario, the optimum beam is chosen with four update period: 20, 40, 80, and 160 ms. The same periods are used in the case of beam sweeping for comparison. All vehicles drive at a constant speed of 100 km/h and they report their position every 200 ms with an accuracy of 2 m. Fig. 8 shows how the average SINR evolves for each case. On the one hand, the proposed beam optimization method outperforms the beam sweeping strategy for all beam update periods, especially when this value is increased, with up to 0.4 dB more SINR in average. The optimum beam considering both ICI and vehicle positioning also showcases a much more stable performance as the time between beam updates increases. On the other hand, it is of interest to evaluate the system-level performance in terms of beam outage probability. Again, the proposed beam optimization presents a very stable behavior as seen in Fig. 9, with values always below a 0.2. The beam sweeping approach, with high use ratio of very narrow beams, shows an slightly increased probability of beam outage for higher beam update periods.

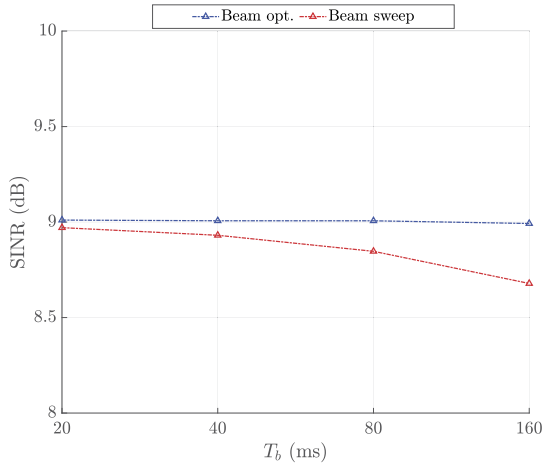

Fig. 8. Average SINR for different beam update periods.

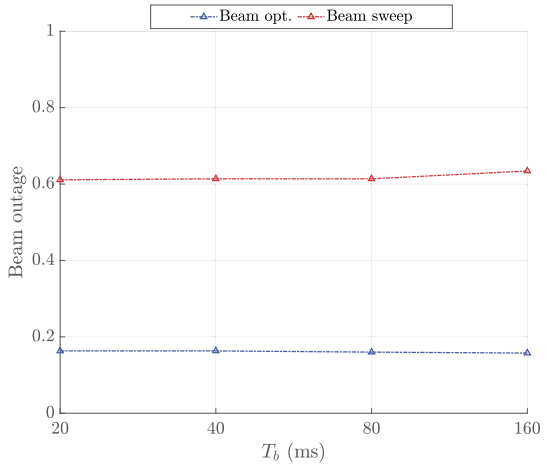

Fig. 9. Outage probability for different beam update periods.

4.4. Comparison with other optimization methods

In order to evaluate the optimality of the proposed approach, it is compared to two different optimization algorithms. For a given beam update period (40 ms) and positioning accuracy (2 m), a subset of 10 vehicles is used to extract some quality parameters for two other optimization methods and compare them with the abovementioned results. In particular, the two chosen algorithms are: a global search with sequential quadratic programming (SQP) [38,39] and the genetic algorithm (GA) [40]. The former makes use of a large number of starting points to iteratively solve individual

Table 2
Performance comparison between the three optimization methods.

Parameter	Beamset	SQP	GA
Avg. SINR (dB)	7.37	8.46	8.44
Avg. P_{bo}	0.02	0.24	0.19
Avg. Time (norm.)	1	402	830
Avg. $\Delta\theta_{-3\,\mathrm{dB}}$ (deg.)	–	6.78	6.37
Avg. $\Delta\phi_{-3\,\mathrm{dB}}$ (deg.)	–	13.0	12.83

problems. It allows to solve non-linear constrained problems, as it is the case. The optimization variables (beamwidth in azimuth and elevation) are restricted to a range of values and the maximization function is far from presenting a linear behavior. The second method, GA, is based on a natural-selection process, creating random children at each iteration from a subset of the parents in the previous stage. When the population and iterations are large enough, the solution converges to the optimum. The following settings are applied to both optimization methods:

- A total number of 500 trial points are initially used in the global search, which are reduced to 200 in successive iterations.
- The tolerance of the SQP and GA optimizer variables (beamwidth) is set to 0.01°.
- No thread parallelization is used in the optimization, which could partially alleviate the time consumption.

Table 2 presents the results for a subset of 10 vehicles with positions ranging between 150 and 250 m along their trajectories. The distance criterion is used in order to obtain meaningful mean values of SINR and outage, since it does not make sense to average power for very distinct distances between transmitter and receiver. The average calculation time for each optimization (normalized to the original beam search) and the average difference between the optimum beamwidth and the one chosen from the beamset are also given. As it can be stated, the use of optimization algorithms improves the achievable SINR at the expense of much larger computation times. Regarding the beam outage probability, it is much larger for the optimum beams as well, since they tend to lower beamwidth values. The goal function for the entire trajectory is maximized but it does not imply that all points are maximum. Additionally, being out of the beam does not necessarily mean that the received power is insufficient for an adequate decoding of data. For such analysis, higher layers should be implemented to calculate other parameters such as the packet error rate (PER).

5. Conclusion

This paper addresses the optimization of the antenna beamwidth in high-mobility V2N communication scenarios using massive antenna arrays at mmWave band. In particular, the information of the vehicle speed and position, assuming a certain error, are used to estimate the channel performance along the vehicle trajectory in terms of SINR and outage probability to optimize the antenna beam width. Analytical expressions are provided to estimate the ICI depending on the Doppler shift due to the vehicle speed and the accuracy when positioning the car in the scenario. The results are also compared to those obtained with a hierarchical beamset codebook in which the beam is refined after an initial tracking phase.

An increased performance in terms of SINR and throughput is shown when the antenna beamwidth is adapted according to the vehicle dynamics compared to the wide-spread beam sweeping case. This is true even when a finite beamset is chosen, equal to the one used in beam sweeping. The main constraint of the proposed methodology concerns the accuracy when estimating the user trajectory but this is compensated in the optimization at the expense of reduced antenna gains. SINR and throughput are maximized when the vehicle position is known with better accuracy, whereas gain drops due to beam misalignment do not always follow this trend. Nevertheless, a loss smaller than 3 dB is given at least for 94% of the cases. The discussed optimization method also presents a very stable performance with beam update periods ranging from 20 to 160 ms.

Declaration of competing interest

The authors declare that they have no known competing financial interests or personal relationships that could have appeared to influence the work reported in this paper.

Acknowledgement

This work was partly funded by the Spanish Ministerio de Economía y Competitividad under the projects PID2019-107885GB-C31 and MDM2016-0600, the Catalan Research Group 2017 SGR 219, and “Industrial Doctorate” programme of the Agència de Gestió d’Ajuts Universitaris i de Recerca (2018-DI-084). The Spanish Ministerio de Universidades contributes via a predoctoral grant to the first author (FPU17/05561).

Appendix A

In [41], Bello justified that, under slow-fading condition, one can define the channel fading terms by the two first terms of its series expansion. In 5G FR2 communications, the symbol period, T, is 16.67 μs at most ($\Delta f = 60\,kHz$). Moreover, according to the calculations in [6,29], typical values of the channel coherence time in mmWave V2I communications are strictly more than 1 ms. Hence, slow-fading condition is assumed to be fulfilled and the channel coefficients for the k-th subcarrier are expressed as:

$$h_k(t) = h_k(t_0) + h'_k(t_0)(t - t_0)\,. \tag{A.1}$$

The received signal in time, defined in (10), corresponds to the addition of all subcarrier symbols, that combined with (A.1) lead to the following expression:

$$\begin{aligned} r(t) = &\frac{1}{\sqrt{NT}} \sum_{k=1}^{N} h_k(t_0) x_k e^{j2\pi f_k t} \\ &+ \frac{1}{\sqrt{NT}} \sum_{k=1}^{N} h'_k(t_0)(t - t_0) x_k e^{j2\pi f_k t} + n(t)\,. \end{aligned} \tag{A.2}$$

Then, the output of the k-th correlator is the one defined in (11). The three addends in (11) correspond to the signal, ICI and noise components. First, the symbol to be detected has a power, namely P, that is proportional to the transmit power divided by the channel path loss. The power perceived by the receiver will scale accordingly to the position with respect to the beam footprint. Assuming that the BS focuses to the estimated position of the vehicle, there will be a decrease of the signal strength mainly due to two factors: the error in positioning and the vehicle movement.

The second term in (A.2) must be carefully depicted, since both the beamforming antenna (gain and misalignment) and user movement (Doppler) influence the ICI power in different ways. The power of the ICI is then computed as

Table A.3
Definition of terms in (A.5) for $\tau = 0$.

Variable	Definition
C	$e^{k_\theta(\cos\Delta\theta_\varepsilon - 1) + k_\phi(\cos\Delta\phi_\varepsilon - 1)}$
A_1'	$\frac{1}{2}k_\theta \sin(\Delta\theta_\varepsilon)\Delta\theta'$
A_2'	$\frac{1}{2}k_\phi \sin(\Delta\phi_\varepsilon)\Delta\phi'$
B'	$-j2\pi f_D \cos\theta_0 \cos\phi_0$
$\Delta\theta'$	$\frac{hv(\tan^2(\theta_0)+1)\cos\theta_0}{(D_0\cos\theta_0 + h\tan\theta_0)^2}$
$\Delta\phi'$	$\frac{v\sin(\theta_0)}{D_0\cos\theta_0}$
A_1''	$(A_1')^2 + \frac{1}{2}k_\theta \sin(\Delta\theta_\varepsilon)\Delta\theta''$
A_2''	$(A_2')^2 + \frac{1}{2}k_\phi \sin(\Delta\phi_\varepsilon)\Delta\phi''$
B''	$B' - j8\pi f_D\Big[\sin\theta_0\cos\phi_0\Delta\theta' + \cos(\theta_0)\sin\phi_0\Delta\phi'\Big]^2$
$\Delta\theta''$	$\frac{2hv^2(\tan^2\theta_0+1)\cos^2\phi_0}{(D_0\cos\theta 0 + h\tan\theta_0)^3}$
$\Delta\phi''$	$\frac{2v^2\sin\phi_0\cos\phi_0}{(D_0\cos\theta_0)^2}$
D_0	$D\frac{\cos\theta_{\text{LOS}}\sin(\phi_{\text{LOS}}-\alpha)}{\cos\theta_0\sin(\phi_0-\alpha)}$

$$I_k = \mathbb{E}\left[\left|\frac{NT}{j2\pi}\sum_{\substack{l=1\\l\neq l}}^{N}\frac{h_l'(t_0)x_l}{l-k}\right|^2\right] = I_1 + I_2 \tag{A.3}$$

and it is decomposed in two parts, being I_1 the crossed terms correlation and I_2, the self-correlation of all the undesired symbols at the i-th branch. Given zero-mean i.i.d. symbols, $I_1 = 0$ and only the second term remains in the equation:

$$\begin{aligned} I_k = I_2 &= \Big(\frac{NT}{2\pi}\Big)^2 \sum_{\substack{l=1\\l\neq k}}^{N}\frac{1}{(l-k)^2}E[|h_l'(t_0)x_l|^2] \\ &= |R_1''(0)|P\Big(\frac{NT}{2\pi}\Big)^2\sum_{\substack{l=1\\l\neq k}}^{N}\frac{1}{(l-k)^2}, \end{aligned} \tag{A.4}$$

where $R_1''(0)$ is the second derivative of the self-correlation function particularized for $\tau = 0$.

In (8), the temporal correlation of the LOS component is detailed. Both positioning and movement errors influence the channel correlation in magnitude and phase. The angles are referred with respect to the axes defined by the driving direction and the zenith. The bivariant von Mises distribution [33] is used to model the beam pattern, which extends the initial approach in [29] to both angular dimensions, and the two variables are assumed to be uncorrelated.

For $\tau = 0$, the second derivative of R_1 can be expressed in the following form:

$$R_1''(0) = \mathbb{E}\Big[C\big(A_1'' + 2A_1'A_2' + A_2'' + 2A_1'B' + 2A_2'B' + B''\big)\Big] \tag{A.5}$$

and each term is detailed in Table A.3. The undefined parameters are: v stands for the magnitude of the velocity vector, D is the LOS distance between the BS and the vehicle at the reported position and h is the height difference between both.

Considering a noise power that scales with the sub-channel bandwidth, $N_0\Delta f$, the SINR of the i-th subcarrier follows the expression detailed in (12).

References

[1] A. Pfadler, G. Jornod, A.E. Assaad, P. Jung, Predictive quality of service: adaptation of platoon inter-vehicle distance to packet inter-reception time, in: 2020 IEEE 91st Vehicular Technology Conference (VTC2020-Spring), 2020, pp. 1–5.

[2] A. Kousaridas, R.P. Manjunath, J. Perdomo, C. Zhou, E. Zielinski, S. Schmitz, A. Pfadler, Qos prediction for 5g connected and automated driving, IEEE Commun. Mag. 59 (9) (2021) 58–64, https://doi.org/10.1109/MCOM.110.2100042.

[3] S. Euler, A. Pfadler, L. Fernández Ferreira, H. Zhao, Spectrum needs of cooperative, connected and automated mobility, in: 2021 IEEE 93st Vehicular Technology Conference (VTC2021-Spring), 2021, pp. 1–6.

[4] T.E. Bogale, Adaptive beamforming and modulation design for 5G V2I networks, in: 2020 10th Annual Computing and Communication Workshop and Conference (CCWC), 2020, pp. 0090–0096.

[5] M. Matalatala, M. Deruyck, E. Tanghe, L. Martens, W. Joseph, Simulations of beamforming performance and energy efficiency for 5G mm-wave cellular networks, in: 2018 IEEE Wireless Communications and Networking Conference (WCNC), 2018, pp. 1–6.

[6] A. Pfadler, C. Ballesteros, J. Romeu, L. Jofre, Hybrid massive MIMO for urban V2I: sub-6 GHz vs mmWave performance assessment, IEEE Trans. Veh. Technol. 69 (5) (2020) 4652–4662, https://doi.org/10.1109/TVT.2020.2982743.

[7] I. Maskulainen, P. Luoto, P. Pirinen, M. Bennis, K. Horneman, M. Latva-aho, Performance evaluation of adaptive beamforming in 5G-V2X networks, in: 2017 European Conference on Networks and Communications (EuCNC), 2017, pp. 1–5.

[8] D. Kong, J. Cao, A. Goulianos, F. Tila, A. Doufexi, A. Nix, V2I mmWave connectivity for highway scenarios, in: 2018 IEEE 29th Annual International Symposium on Personal, Indoor and Mobile Radio Communications (PIMRC), 2018, pp. 111–116.

[9] Y. Wang, K. Venugopal, A.F. Molisch, R.W. Heath, MmWave vehicle-to-infrastructure communication: analysis of urban microcellular networks, IEEE Trans. Veh. Technol. 67 (8) (2018) 7086–7100, https://doi.org/10.1109/TVT.2018.2827259.

[10] M.K. Samimi, T.S. Rappaport, Ultra-wideband statistical channel model for non line of sight millimeter-wave urban channels, in: 2014 IEEE Global Communications Conference, 2014, pp. 3483–3489.

[11] T.S. Rappaport, Y. Xing, G.R. MacCartney, A.F. Molisch, E. Mellios, J. Zhang, Overview of millimeter wave communications for fifth-generation (5G) wireless networks – with a focus on propagation models, IEEE Trans. Antennas Propag. 65 (12) (2017) 6213–6230, https://doi.org/10.1109/TAP.2017.2734243.

[12] C.K. Anjinappa, I. Guvenc, Angular and temporal correlation of V2X channels across sub-6 GHz and mmWave bands, in: 2018 IEEE International Conference on Communications Workshops (ICC Workshops), 2018, pp. 1–6.

[13] K. Guan, B. Ai, B. Peng, D. He, G. Li, J. Yang, Z. Zhong, T. Kürner, Towards realistic high-speed train channels at 5G millimeter-wave band—part I: paradigm, significance analysis, and scenario reconstruction, IEEE Trans. Veh. Technol. 67 (10) (2018) 9112–9128, https://doi.org/10.1109/TVT.2018.2865498.

[14] J. Lorca, M. Hunukumbure, Y. Wang, On overcoming the impact of Doppler spectrum in millimeter-wave V2I communications, in: 2017 IEEE Globecom Workshops (GC Wkshps), 2017, pp. 1–6.

[15] J.A. del Peral-Rosado, R. Raulefs, J.A. López-Salcedo, G. Seco-Granados, Survey of cellular mobile radio localization methods: from 1G to 5G, IEEE Commun. Surv. Tutor. 20 (2) (2018) 1124–1148.

[16] G.M. Hoang, B. Denis, J. Härri, D. Slock, et al., Distributed link selection and data fusion for cooperative positioning in GPS-aided IEEE 802.11 p VANETs, Proc. WPNC 15 (2015) 1–6.

[17] G.E. Garcia, G. Seco-Granados, E. Karipidis, H. Wymeersch, Transmitter beam selection in millimeter-wave MIMO with in-band position-aiding, IEEE Trans. Wirel. Commun. 17 (9) (2018) 6082–6092.

[18] H. Wymeersch, G. Seco-Granados, G. Destino, D. Dardari, F. Tufvesson, 5G mmWave positioning for vehicular networks, IEEE Wirel. Commun. 24 (6) (2017) 80–86.

[19] T. Shimizu, V. Va, G. Bansal, R.W. Heath, Millimeter wave V2X communications: use cases and design considerations of beam management, in: 2018 Asia-Pacific Microwave Conference (APMC), IEEE, 2018, pp. 183–185.

[20] N. Garcia, H. Wymeersch, E.G. Ström, D. Slock, Location-aided mm-wave channel estimation for vehicular communication, in: 2016 IEEE 17th International Workshop on Signal Processing Advances in Wireless Communications (SPAWC), IEEE, 2016, pp. 1–5.

[21] I.E.E.E. Std, 802.15.3c-2009 (Amendment to IEEE Std 802.15.3-2003), IEEE Standard for Information Technology – Telecommunications and Information Exchange between Systems – Local and Metropolitan Area Networks – Specific Requirements. Part 15.3: Wireless Medium Access Control (MAC) and Physical Layer (PHY) Specifications for High Rate Wireless Personal Area Networks (WPANs) Amendment 2: Millimeter-Wave-Based Alternative Physical Layer Extension, Oct. 2009.

[22] V. Va, T. Shimizu, G. Bansal, R.W. Heath, Beam design for beam switching based millimeter wave vehicle-to-infrastructure communications, in: 2016 IEEE International Conference on Communications (ICC), IEEE, 2016, pp. 1–6.

[23] Y. Kang, H. Seo, W. Choi, Optimal receive beamwidth for time varying vehicular channels, in: 2020 IEEE Wireless Communications and Networking Conference (WCNC), IEEE, 2020, pp. 1–6.
[24] Y. Feng, D. He, Y. Guan, Y. Huang, Y. Xu, Z. Chen, Beamwidth optimization for millimeter-wave V2V communication between neighbor vehicles in highway scenarios, IEEE Access 9 (2021) 4335–4350.
[25] P. Petrus, J.H. Reed, T.S. Rappaport, Effects of directional antennas at the base station on the Doppler spectrum, IEEE Commun. Lett. 1 (2) (1997) 40–42.
[26] S.J. Nawaz, N.M. Khan, M.N. Patwary, M. Moniri, Effect of directional antenna on the Doppler spectrum in 3-D mobile radio propagation environment, IEEE Trans. Veh. Technol. 60 (7) (2011) 2895–2903.
[27] S. Jaeckel, L. Raschkowski, K. Börner, L. Thiele, QuaDRiGa: a 3-D multi-cell channel model with time evolution for enabling virtual field trials, IEEE Trans. Antennas Propag. 62 (6) (2014) 3242–3256.
[28] Tiejun Wang, J.G. Proakis, E. Masry, J.R. Zeidler, Performance degradation of OFDM systems due to Doppler spreading, IEEE Trans. Wirel. Commun. 5 (6) (2006) 1422–1432.
[29] V. Va, J. Choi, R.W. Heath, The impact of beamwidth on temporal channel variation in vehicular channels and its implications, IEEE Trans. Veh. Technol. 66 (6) (2017) 5014–5029, https://doi.org/10.1109/TVT.2016.2622164.
[30] J.D. Parsons, A.S. Bajwa, Wideband characterisation of fading mobile radio channels, IEE Proc. F, Commun. Radar Signal Process. 129 (2) (1982) 95.
[31] R.H. Clarke, A statistical theory of mobile-radio reception, Bell Syst. Tech. J. 47 (6) (1968) 957–1000.
[32] W.C. Jakes, D.C. Cox, Microwave Mobile Communications, Wiley-IEEE Press, 1994.
[33] K.V. Mardia, G. Hughes, C.C. Taylor, H. Singh, A multivariate von Mises distribution with applications to bioinformatics, Can. J. Stat. 36 (1) (2008) 99–109.
[34] M.-D. Kim, J. Liang, J. Lee, J. Park, B. Park, H.K. Chung, Investigating the effect of antenna beamwidth on millimeter-wave channel characterization, in: 2016 URSI Asia-Pacific Radio Science Conference (URSI AP-RASC), 2016, pp. 1–4.
[35] Z. Hanzaz, H.D. Schotten, Analysis of effective SINR mapping models for MIMO OFDM in LTE system, in: 2013 9th International Wireless Communications and Mobile Computing Conference (IWCMC), 2013, pp. 1509–1515.
[36] Technical 3GPP, Specification Group Radio Access Network; Study on Evaluation Methodology of New Vehicle-to-Everything (V2X) Use Cases for LTE and NR; (Release 15), Technical Report (TR) 37.885, 3rd Generation Partnership Project (3GPP), version 15.3.0, June 2019.
[37] 3GPP, Technical Specification Group Radio Access Network; NR; Physical channels and modulation; (Release 16), Technical Specification (TS) 38.211, 3rd Generation Partnership Project (3GPP), version 16.3.0, September 2020.
[38] Z. Ugray, L. Lasdon, J. Plummer, F. Glover, J. Kelly, R. Martí, Scatter Search and Local NLP Solvers: A Multistart Framework for Global Optimization, vol. 19, 2007.
[39] J. Nocedal, S. Wright, Numerical Optimization, Springer Science & Business Media, 2006.
[40] D.E. Goldberg, Genetic Algorithms in Search, Optimization, and Machine Learning, Addison, Addison-Wesley, 1989.
[41] P. Bello, Characterization of randomly time-variant linear channels, IEEE Trans. Commun. Syst. 11 (4) (1963) 360–393.